Experimental and Computational Studies of High-Valent Nickel and Palladium Complexes

Nicole M. Camasso,[†] Allan J. Canty,*[,‡] Alireza Ariafard,[‡] and Melanie S. Sanford*[,†]

[†]Department of Chemistry, University of Michigan, 930 N University Ave, Ann Arbor, MI 48109, USA

[‡]School of Physical Sciences, University of Tasmania, Hobart, Tasmania 7001, Australia

Supporting Information Placeholder

ABSTRACT: This Article describes a detailed comparison of the organometallic chemistry of high-valent nickel and palladium model complexes supported by tris(pyrazolyl)borate and cycloneophyl ligands. The accessibility of the M^{III} and M^{IV} oxidation states with each metal is investigated through electrochemical and chemical oxidation of the M^{II} precursors. These studies show that the Ni^{II} precursor readily undergoes both one- and two-electron oxidations to generate stable Ni^{III} and Ni^{IV} products. In contrast, under the conditions examined, the Pd^{II} analogue undergoes exclusively two-electron oxidation reactions to form Pd^{IV}. Reactivity studies of isolated Ni^{IV} and Pd^{IV} complexes show that both participate in $C(sp^3)$–heteroatom coupling reactions and that the reactions at Ni^{IV} are approximately two orders of magnitude faster than those at Pd^{IV}. Experimental and computational mechanistic studies implicate outer-sphere S_N2-type pathways for these processes. With most nucleophiles (e.g., phenoxide, acetate, thiophenoxide), the $C(sp^3)$–heteroatom coupling reaction yields a $TpM^{II}(\sigma\text{-aryl})$ product. However, with azide as the nucleophile, the Ni^{II} product of initial $C(sp^3)$–N_3 coupling undergoes a subsequent $C(sp^2)$–N insertion reaction. Computations implicate an anionic Ni^{III}-nitrene intermediate in this process and show that the Pd analogue of this species is a much higher energy species. Overall, the combined experimental and computational studies demonstrate remarkable similarities in the chemistry of Ni^{IV} and Pd^{IV}, but an enhanced role for Ni^{III} in enabling reactivity that is distinct from that of palladium.

INTRODUCTION

Over the past several decades, fundamental organometallic studies of high-valent Pd complexes have helped to establish that Pd^{IV} intermediates play a key role in a variety of important transformations.[1,2] This work has demonstrated that Pd^{IV} can be accessed under mild reaction conditions using a diverse suite of two-electron oxidants.[1,2] Furthermore, the Pd^{IV} intermediates can undergo challenging reductive elimination reactions that are often complementary to those occurring from Pd^{II} centers.[1,2,3] While Pd^{III} complexes are less common in the literature, studies by Ritter, Mirica, and others have demonstrated the competency of both monomeric and dimeric Pd^{III} intermediates for mediating carbon–carbon and carbon–heteroatom bond-forming reactions.[4] Overall, these fundamental studies have driven advances in the field of high-valent Pd catalysis, which is now widely used for transformations such as C–H functionalization and alkene difunctionalization.[5]

In recent years, tremendous progress has also been made in the field of nickel catalysis.[6] In addition to being a sustainable and low-cost alternative to palladium, new developments in organonickel chemistry have demonstrated that nickel enables transformations that are often not accessible with palladium (e.g., cross-coupling reactions that utilize tertiary alkyl halides[7] or phenol derivatives[8] as electrophiles).[9] However, in comparison to Pd, the organometallic chemistry of high-valent Ni remains underdeveloped. Our lab[10] and others[11,12] have begun to investigate the synthesis and reactivity of organometallic Ni^{III} and Ni^{IV} complexes, and these investigations have provided support for their involvement in challenging bond-forming reactions. However, despite these contributions, very little work has directly compared the relative reactivity of high-valent Ni to that of its group 10 congener, Pd.[6g,13] A systematic comparison of the organometallic chemistry of high-valent Ni to the more established chemistry of high-valent Pd would provide insights into the similarities and differences between these systems. This could ultimately inform the rational development of new group 10 metal-catalyzed reactions.

This Article describes a detailed comparison of the organometallic chemistry of high-valent Pd and Ni complexes bearing tris(pyrazolyl)borate (Tp) and cycloneophyl ligands (Figure 1). We systematically investigate: (i) the accessibility of high-valent Pd (Pd^{IV} and/or Pd^{III}) complexes relative to their Ni analogues; (ii) the relative reactivity and selectivity of carbon-carbon and carbon–heteroatom bond-forming reactions at Pd^{IV} versus Ni^{IV}; and (iii) the mechanistic pathways of these C–C/C–X coupling reactions. Overall, our experimental and computational studies demonstrate that Ni undergoes one-electron redox chemistry more readily than Pd to access isolable Ni^{III} and Ni^{IV} species. The accessibility of these distinct oxidation states enables transformations and mechanistic pathways not seen at the palladium analogues.

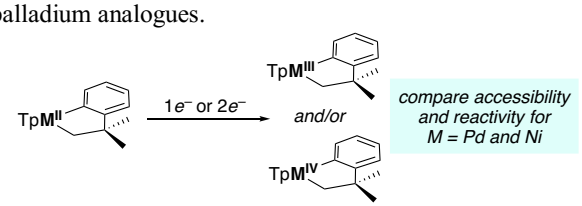

Figure 1. Proposed model systems of analogous high-valent Pd and Ni model complexes

RESULTS AND DISCUSSION

Electrochemistry. We first studied the accessibility of high-valent Ni and Pd complexes by comparing the electrochemistry of the M^{II} complexes **1-Ni** and **1-Pd**. Prior studies from our group[1r,10c-g,14] and others[12g,15] have demonstrated that tris(pyrazolyl)borate (Tp) and cycloneophyl ligands are particularly stabilizing to high-valent group 10 metal complexes. Thus, we targeted M^{II} complexes bearing these ligands for the investigations described herein. As shown in Scheme 1a, complex **1-Ni** was obtained in 93% yield from the reaction of $(PMe_3)_2Ni^{II}(CH_2CMe_2\text{-}o\text{-}C_6H_4)$ with KTp.[10c] Similarly, the treatment of $(COD)Pd(CH_2CMe_2\text{-}o\text{-}C_6H_4)$ (COD = cyclooctadiene) with 1 equiv of NMe_4Tp afforded **1-Pd** in 89% isolated yield (Scheme 1b).

Scheme 1. Synthesis of M^{II} Precursors (a) $K[(Tp)Ni^{II}(CH_2CMe_2\text{-}o\text{-}C_6H_4)]$ (**1-Ni**) and (b) $NMe_4[(Tp)Pd^{II}(CH_2CMe_2\text{-}o\text{-}C_6H_4)]$ (**1-Pd**)

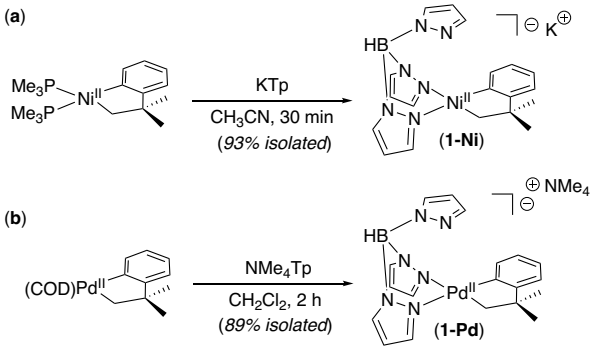

Figure 2 displays the cyclic voltammograms (CVs) of **1-Ni** and **1-Pd** in acetonitrile with tetrabutylammonium hexafluorophosphate (NBu_4PF_6) as the supporting electrolyte. The CV of **1-Ni** reveals two quasi-reversible redox couples with onset poentials of approximately –1.1 V and +0.10 V versus Fc/Fc^+. We assign these to the $Ni^{II/III}$ and $Ni^{III/IV}$ couples, respectively. Notably, the onset potential associated with the $Ni^{II/III}$ couple is among the lowest reported for an organometallic Ni^{III} complex. This is likely due to the strong electron-donor properties of the Tp and cycloneophyl ligands.[16] The observation of two distinct redox couples in this system highlights the propensity of nickel to undergo single electron transfer chemistry.

In comparison, the CV of Pd^{II} complex **1-Pd** (Figure 2) shows a single oxidation wave with an onset potential of approximately –0.10 V, along with a corresponding reduction at –0.80 V vs. Fc/Fc^+. We assign these features to a $Pd^{II/IV}$ redox couple. CVs showing net two electron transfer processes have been reported previously for *mer*-coordinated Pt complexes and related Pd complexes.[17,18] The propensity for two-electron redox at Pd^{II} and Pt^{II} has been attributed to the instability of the corresponding M^{III} species.[17–19]

The large peak separation between the most positive oxidation and reduction waves in both CVs can be rationalized based on the molecular reorganization that accompanies an octahedral/square-pyramidal or octahedral/square planar interconversion.[17,18,20] Overall, the CVs of **1-Ni** and **1-Pd** suggest that while Ni can access distinct one-electron redox pathways, the analogous Pd^{II} complex preferentially undergoes two-electron redox events. Moreover, while the +4 oxidation states of Ni and Pd can be accessed at relatively similar onset potentials (approximately +0.10 V and –0.10 V, respectively), the $Ni^{II/III}$ redox event occurs at a significantly lower onset potential (approximately –1.1 V). The difference between the accessibilities of the high-oxidation states for nickel and palladium mirror the trends seen in the literature, in which Pd^{IV} and Ni^{III} complexes are more common than their Pd^{III} and Ni^{IV} counterparts.[1,4,10–12]

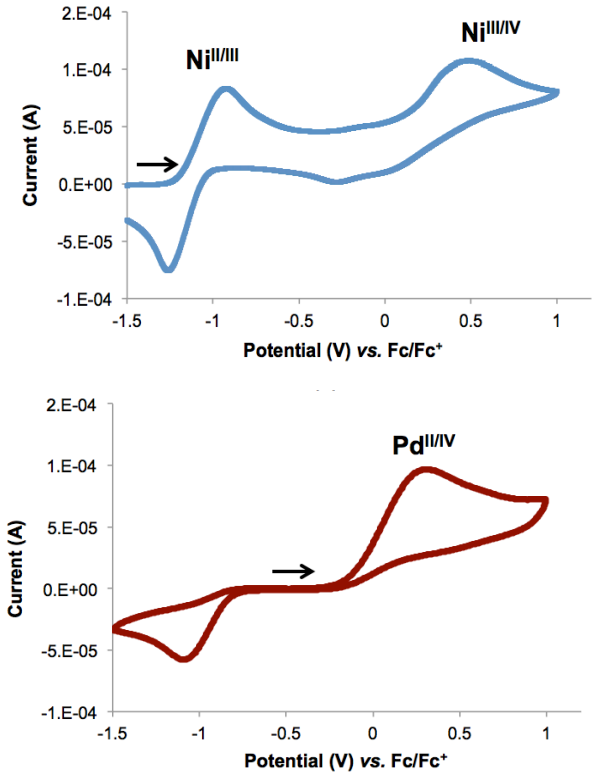

Figure 2. Cyclic Voltammograms of M^{II} Precursors **1-Ni** and **1-Pd**. Conditions: [Ni] = 0.01 M in MeCN, $[NBu_4PF_6]$ = 0.1 M, Scan Rate = 100 mV/s; [Pd] = 0.005 M in MeCN/pyr, $[NBu_4PF_6]$ = 0.1 M, Scan Rate = 100 mV/s.

Chemical Oxidations. The chemical oxidation of **1-Ni** and **1-Pd** was next evaluated using acetylferrocenium tetrafluoroborate ($AcFcBF_4$) as an outer sphere one-electron oxidant. This oxidant was selected due to its suitable redox potential (E^0 = +0.27 V versus Fc/Fc^+) as well as its high solubility under the reaction conditions.[21] The treatment of **1-Ni** with 1 equiv of $AcFcBF_4$ resulted in complete consumption of the diamagnetic Ni^{II} starting material and the formation of ^1H and ^{11}B NMR signals consistent with a paramagnetic product (Figure 3). The observed resonances correspond to those that were previously repoted for the Ni^{III} complex **2-Ni**.[10e,22] In contrast, the use of 2 equiv of $AcFcBF_4$ under otherwise identical conditions resulted in the quantitative formation of a diamagnetic product that we assign as the cationic Ni^{IV} complex **3-Ni** (Figure 3).[23]

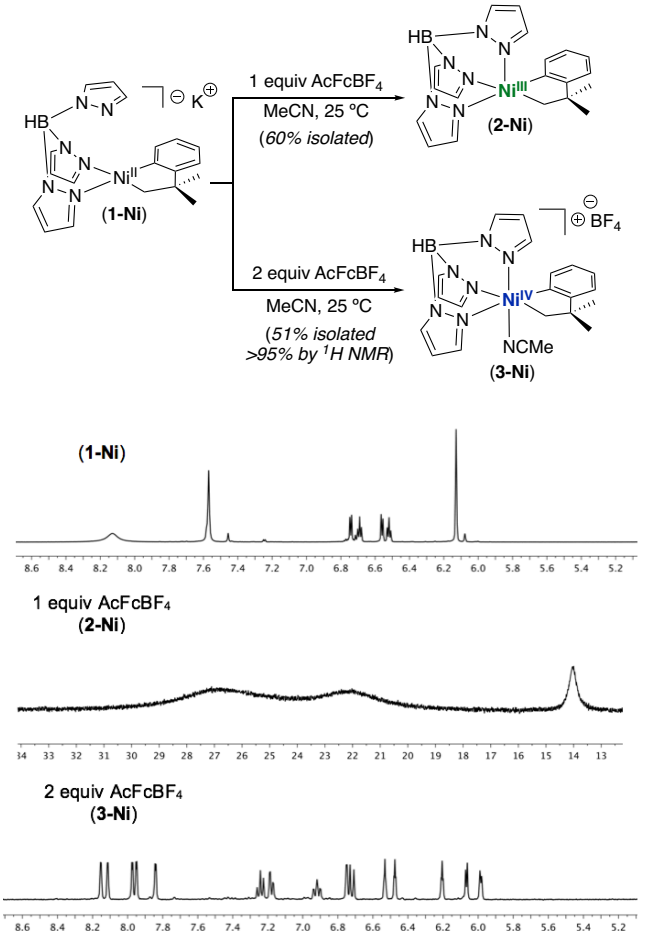

Figure 3. ^{1}H NMR spectra of the reaction of **1-Ni** with 1 or 2 equiv of $AcFcBF_4$, generating the paramagnetic Ni^{III} complex **2-Ni** or the diamagnetic Ni^{IV} complex **3-Ni**

We next examined the analogous chemical oxidations of **1-Pd**. The treatment of **1-Pd** with 2 equiv of $AcFcBF_4$ in MeCN led to a complex mixture of products. However, the addition of 5 equiv of pyridine-d_5 to this reaction resulted in the formation of the cationic pyridine-ligated Pd^{IV} complex **3-Pd** in quantitative yield as determined by ^{1}H NMR spectroscopy (Figure 4).[24] The pyridine ligand appears to stabilize the octahedral Pd^{IV} product. The treatment of **1-Pd** with 1 equiv of $AcFcBF_4$ under otherwise identical conditions resulted in a 50 : 50 mixture of Pd^{IV} complex **3-Pd** and the unreacted Pd^{II} starting material **1-Pd** (Figure 4). In marked contrast to the Ni system in Figure 3, no evidence for Pd^{III} products/intermediates was observed by NMR or EPR spectroscopy. This observation is consistent with the CV of **1-Pd**, which suggests the propensity of this Pd complex to undergo selective two-electron oxidation events.

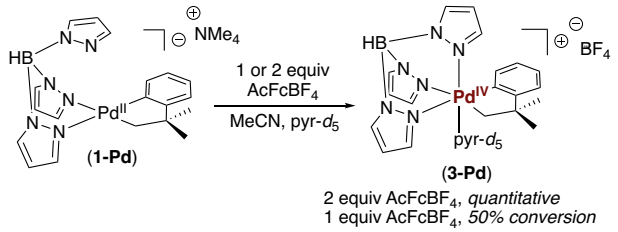

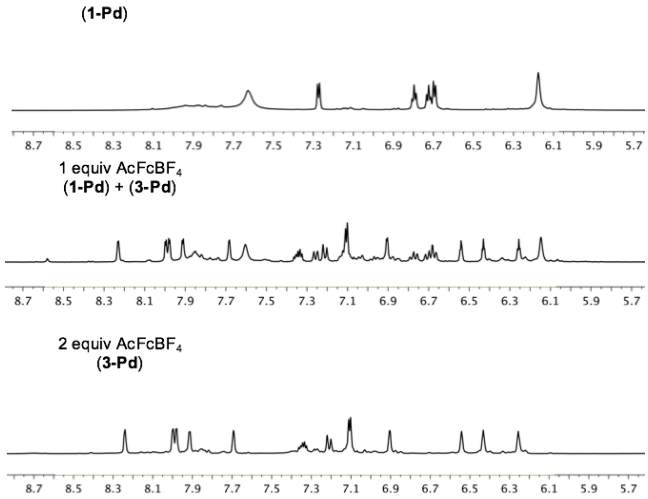

Figure 4. ^{1}H NMR spectra of the reaction of **1-Pd** with 1 or 2 equiv of $AcFcBF_4$

Comparison of Ni^{IV} and Pd^{IV} (Synthesis and Characterization). The oxidation reactions shown in Figures 3 and 4 provide evidence that the combination of the Tp and cycloneophyl ligands support both Ni^{IV} and Pd^{IV} species. However, efforts to study the reactivity of the cationic M^{IV} complexes **3-Ni** and **3-Pd** were complicated by the presence of labile solvent ligands as well as the propensity of **3-Pd** to decompose into complex mixtures of products. As such, we next pursued neutral analogues of **3-Ni** and **3-Pd** containing the trifluoromethyl ligand in order to conduct a detailed comparison of the structures and reactivities of the Pd^{IV} and Ni^{IV} congeners.

The neutral Ni^{IV} trifluoromethyl complex **4-Ni** was prepared via the treatment of **1-Ni** with the electrophilic trifluoromethylating reagent, *S*-(trifluoromethyl)dibenzothiophenium triflate (Umemoto's reagent), and subsequent purification by silica gel chromatography (Scheme 2a).[10c] The Pd analogue **4-Pd** was prepared from Pd^{II} precursor **1-Pd** via a similar procedure (Scheme 2b). Complexes **4-Ni** and **4-Pd** were characterized by ^{1}H, ^{13}C, ^{11}B, and ^{19}F NMR spectroscopy. The ^{1}H NMR spectra of these complexes are remarkably similar, and display resonances consistent with a κ^3-tris(pyrazolyl)borate ligand bound to an octahedral M^{IV} center. One notable difference between the two spectra is the chemical shift of the diastereotopic methylene protons in **4-Ni** (two resonances between 4.7-4.9 ppm) and **4-Pd** (two resonances between 4.1-4.2 ppm). The greater deshielding of the α-protons in **4-Ni** suggest a comparatively more electrophilic M^{IV}–σ-alkyl carbon.

Scheme 2. Synthesis of (a) **4-Ni** and (b) **4-Pd**

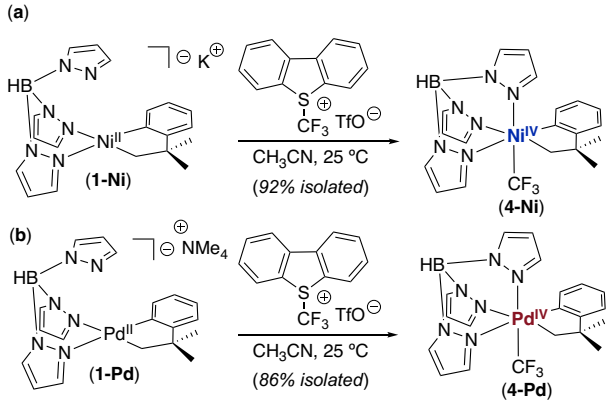

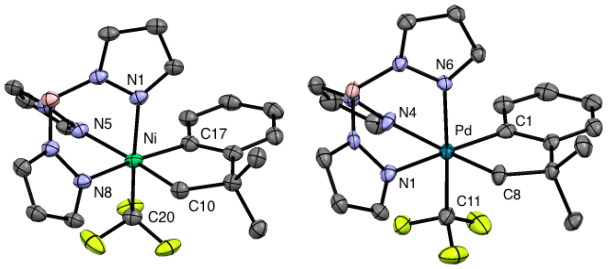

Figure 5. ORTEP diagrams of (a) **4-Ni** and (b) **4-Pd.** Thermal ellipsoids are drawn at 50% probability. Hydrogen atoms and disorder in the trifluoromethyl group of **4-Pd** have been omitted for clarity.

Crystals of **4-Ni** were obtained by slow evaporation of a methanol solution, while those of **4-Pd** were obtained from a concentrated acetone solution. The solid-state structure of each complex is shown in Figure 5. The Tp ligand binds κ^3 to both metal centers, forming the anticipated octahedral geometries. The Pd analogue has significantly longer bond distances, as is expected for a second-row versus a first-row transition metal.[25] For example, the Pd–CF_3 bond length (2.036 Å) is approximately 0.1 Å longer than that of the Ni analogue (1.941 Å), and is comparable to that of related Pd^{IV}–CF_3 complexes reported in the literature.[26,27]

Comparison of Ni^{IV} and Pd^{IV} Reactivity. Heating Ni^{IV} complex **4-Ni** at 70 ºC in MeCN resulted in slow C(sp^3)–C(sp^2) bond-forming reductive elimination to afford benzocyclobutane product, **5** (r_0 = 9.1 x 10^{-9} M/s at 70 ºC with [Ni] = 0.011 M; Scheme 3b). Notably, this reaction proceeds approximately 100-fold slower than the analogous transformation from the cationic Ni^{IV} complex **3-Ni** (r_0 = 9.0 x 10^{-7} M/s at 70 ºC with [Ni] = 0.011 M; Scheme 3a). This is presumably due to stabilization of Ni^{IV} by the CF_3 ligand. As shown in Scheme 4, the Pd^{IV} analogue **4-Pd** proved even more stable and did not undergo detectable C(sp^3)–C(sp^2) bond-forming reductive elimination to form **5** over several weeks at 70 ºC.

Scheme 3. Initial rates data for C(sp^3)–C(sp^2) coupling from (a) **3-Ni** and (b) **4-Ni**

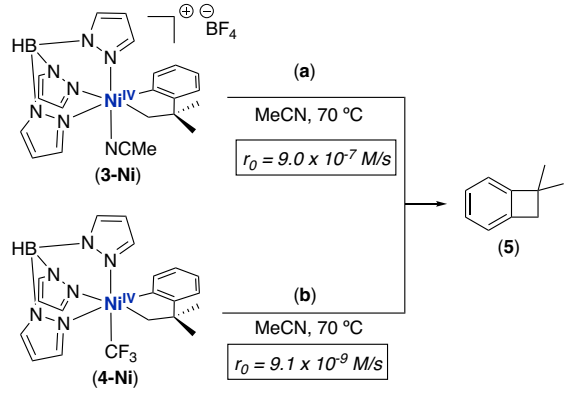

Scheme 4. Complex **4-Pd** is inert to C(sp^3)–C(sp^2) coupling over weeks at 70 ºC

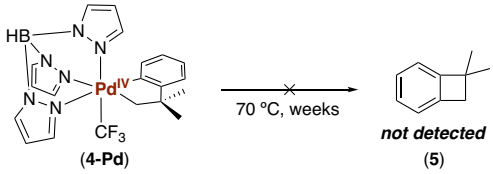

The treatment of **4-Ni** and **4-Pd** with NMe_4X (where X = OAc, OPh, SPh, and N_3) led to highly selective C(sp^3)–heteroatom coupling to form M^{II} products **6a-d** (Scheme 5).[28] No products derived from C(sp^3)–C(sp^2) or C(sp^2)–heteroatom coupling were observed under any of the conditions examined with either Ni or Pd.[29] Kinetic studies show that these reactions are 2nd order overall: first order in [M^{IV}] and first order in [nucleophile]. Plots of the Swain-Scott nucleophilicity parameters (n_x) versus the initial rates of these reactions (r_0) show a linear correlation for both Ni and Pd (0.944 and 0.974, respectively, Figure 6).[30] Overall, these data are consistent with an S_N2-type mechanism for this transformation. This is generally the lowest energy pathway for C(sp^3)–heteroatom couplings from high-valent group 10 metal centers.[14b-e,31]

Scheme 5. C(sp^3)–heteroatom coupling from M^{IV} complexes **4-Ni/Pd** to form M^{II} products **6a-d**. [a]Isolated yield. [b]NMR conversion yield; **6d-Ni** was not sufficiently stable for isolation. [c]NMR conversion yield; reaction required 5 equiv of NR_4X.

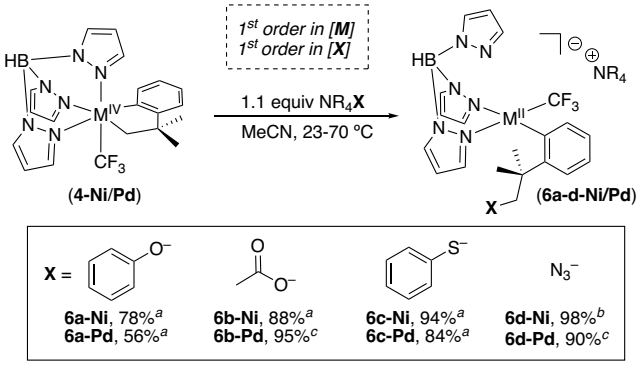

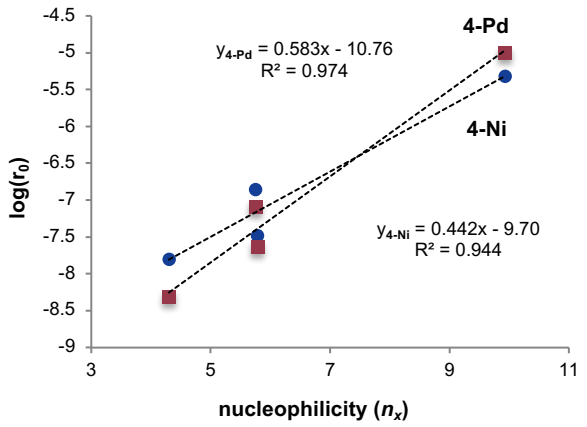

Figure 6. Swain-Scott plot relating the relative nucleophilicities (n_x) with the initial rate (r_0) of C–heteroatom coupling. Starting Conditions: [Ni] = 0.0044 M, [X] = 0.0054 M, T = 23 ºC; [Pd] = 0.011 M, [X] = 0.057 M, T = 60 ºC

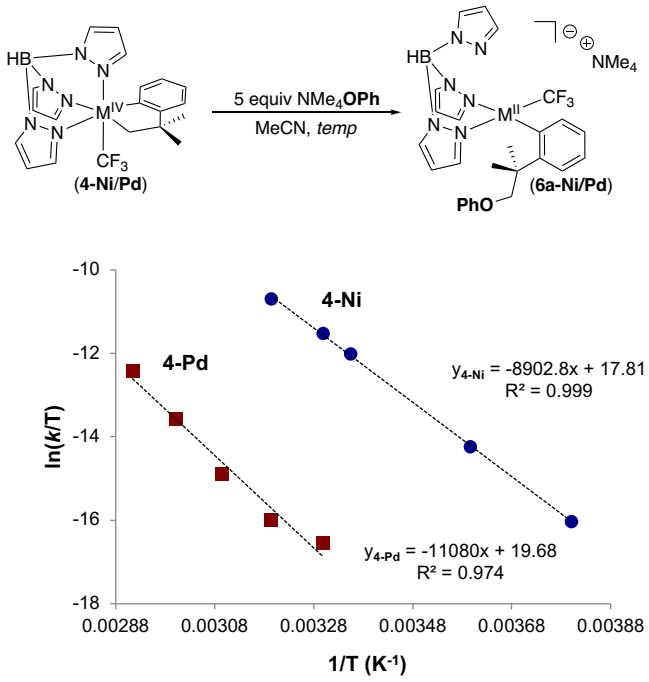

Figure 7. Eyring Plot for C(sp^3)–O Coupling from M^{IV} Complexes **4-Ni** and **4-Pd**. Conditions: [Ni] = 0.011 M, [NMe_4OPh] = 0.055 M, –10 to 40 ºC; [Pd] = 0.011 M, [NMe_4OPh] = 0.055 M, T = 30 to 70 ºC

While **4-Ni** and **4-Pd** exhibit comparable selectivity for C(sp^3)–heteroatom coupling, the rates of these processes differ dramatically as a function of metal. For example, in the presence of 5 equiv of NMe_4OPh, C(sp^3)–O coupling at Ni^{IV} proceeds approximately 2 orders of magnitude faster than the analogous reaction at Pd^{IV} (r_0 = 2.0 x 10^{-6} M/s versus 1.3 x 10^{-8} M/s at 30 ºC; [M] = 0.011 M). The initial rates of C(sp^3)–O bond-formation from **4-Ni** and **4-Pd** were also examined as a function of temperature (for Ni: –10 to 40 ºC; for Pd: 30 to 70 ºC). The resulting Eyring plots are shown in Figure 7, and the activation parameters from this analysis are provided in Table 1. Negative entropy of activation values ($\Delta S^{\ddagger}$) were obtained for both Ni and Pd (–12.0 and –8.09 eu, respectively), indicating fewer degrees of freedom in the transition states for both C(sp^3)–O coupling reactions. These results are further consistent with a mechanism involving nucleophilic attack of phenoxide on the M^{IV}–alkyl carbon.[14d,31] Overall, the Eyring parameters implicate similar pathways for C–O coupling at the two metal centers, with the Pd system being a significantly higher energy process.

Table 1. Activation Parameters for C(sp^3)–O Coupling from **4-Ni** and **4-Pd**

	4-Ni	**4-Pd**
$\Delta H^{\ddagger}$ (kcal/mol)	17.7	22.0
$\Delta S^{\ddagger}$ (cal/mol K)	–12.0	–8.09
$\Delta G_{303K}^{\ddagger}$ (kcal/mol)	21.3	24.5

Computational Studies. The experimental data implicate a mechanism involving S_N2-type attack on the methylene group attached to the M^{IV} center. We next pursued DFT[32,33] calculations to validate this mechanism and to explore several key features of these processes including: (i) whether an open coordination site at M^{IV} is necessary for S_N2-type C–heteroatom coupling and (ii) how the mechanistic pathways and transition states at Pd^{IV} compare to those at Ni^{IV}. At the outset, we noted that similar S_N2-type mechanisms have been proposed for C(sp^3)–heteroatom coupling reactions from other cycloneophyl Pd^{IV} complexes.[14b-e,31] However, in these latter systems, the dissociation of a ligand (usually the nucleophile, X) is typically required prior to nucleophilic attack. Indeed, the vast majority of reductive elimination reactions at Pd^{IV} and Pt^{IV} are believed to occur via five-coordinate intermediates. In the present system, C(sp^3)–heteroatom coupling at M^{IV} complexes **4-Ni** and **4-Pd** could proceed via dissociation of a pyrazole group (pathway A) or by direct nucleophilic attack at the six-coordinate complex (pathway B), a transformation that has much less precedent at octahedral group 10 centers (Figure 8).[34]

Figure 8. Possible mechanisms for carbon–heteroatom coupling from **4-Ni/Pd**

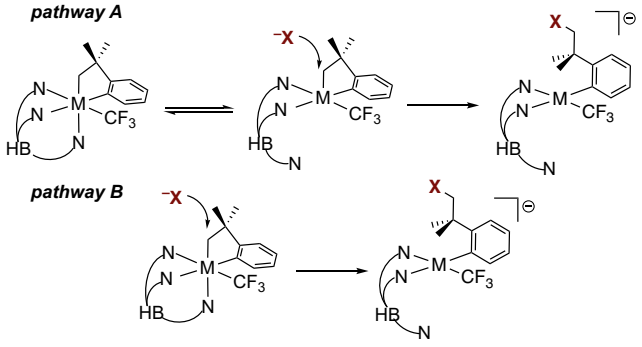

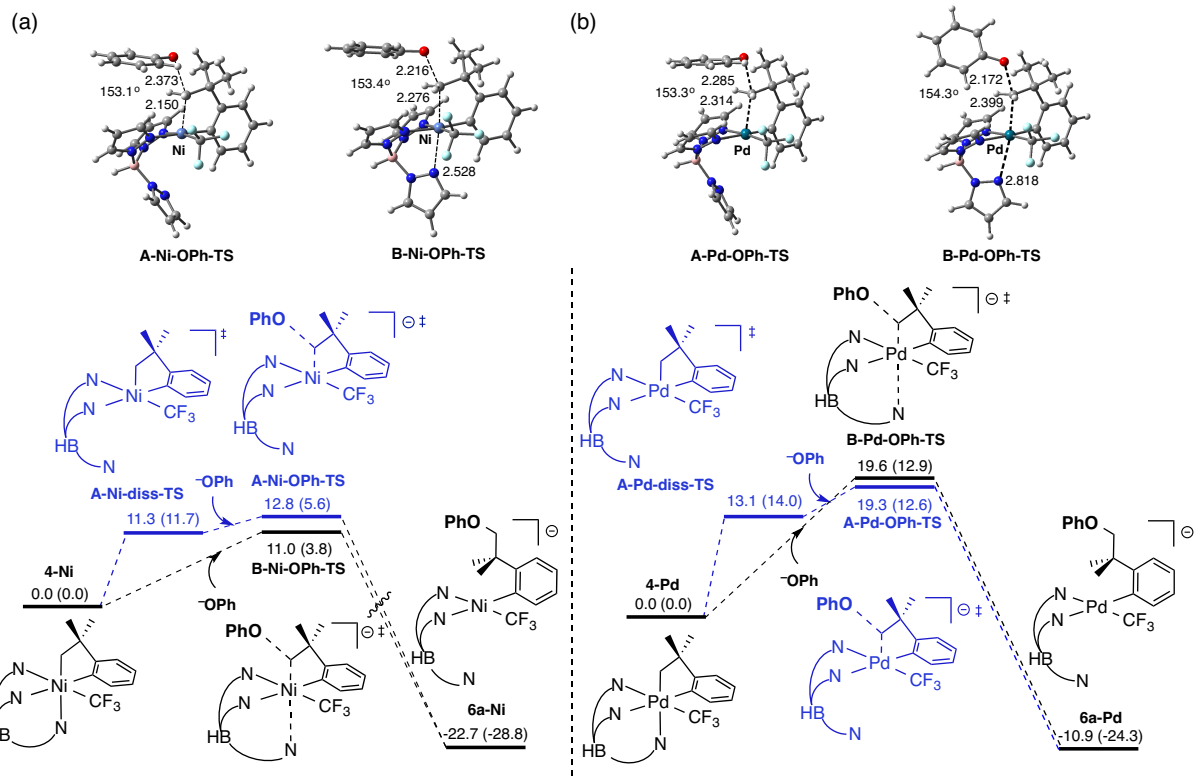

Figure 9. Energy profiles and Gaussview diagrams of the transition states for the reaction of phenoxide with (a) **4-Ni** and (b) **4-Pd** via a five-coordinate intermediate (mechanism A, blue), or direct nucleophilic attack (mechanism B, black). Square-pyramidal species following **A-M-diss-TS** and encounter complexes before **A-M-OPh-TS** are omitted for clarity. Energies ΔG (ΔH) in kcal/mol.

Two S_N2-type transition states for C(sp^3)–X coupling from **4-Ni** and **4-Pd** were examined. The first involves pre-equilibrium dissociation of one pyrazole group to give a five-coordinate M^{IV} center (pathway A). The second involves direct nucleophilic attack on the sp^3-carbon (pathway B). Computations were carried out for X = OPh, OAc, SPh, and N_3, and a summary of the results is provided in Table 2. Reaction coordinates for phenoxide (PhO^-) are also shown as representative examples in Figure 9.

Table 2. Barriers for C(sp^3)–X bond-formation from **4-Ni** and **4-Pd** via pathway A and pathway B. Energies in kcal/mol at 298K.[a]

Nuc (X)		Pathway A (ΔG‡)	Pathway B (ΔG‡)
4-Ni	OPh	12.8	11.0
	OAc	14.7	14.0
	SPh[a]	11.3	7.6
	N_3	13.3	12.1
4-Pd	OPh	19.3	19.6
	OAc	23.9	23.3
	SPh	17.8	18.0
	N_3	20.8	21.5

[a]Activation barrier is dissociation of pz trans to CH_2.

The transition states for C(sp^3)–OPh bond-formation at the Pd^{IV} center via pathways A (19.3 kcal/mol) and B (19.6 kcal/mol) are substantially higher in energy than the analogous processes at Ni^{IV} (12.8 kcal/mol and 11.0 kcal/mol, respectively), consistent with the experimental rates for these processes. In both systems, the barriers for C(sp^3)–OPh coupling via the five-coordinate versus six-coordinate pathways are remarkably similar in energy (for Pd, $\Delta\Delta G^‡$ = 0.3 kcal/mol; for Ni, $\Delta\Delta G^‡$ = 1.8 kcal/mol). This suggests that ligand dissociation to generate a five-coordinate intermediate is not essential for S_N2-type coupling at these Pd^{IV} and Ni^{IV} centers.

The transition structures and mechanistic pathways for the two complexes are more distinct with the more nucleophilic thiophenoxide as the coupling partner (Figure 10). For palladium, the calculations show similar barriers for five-coordinate ($\Delta G^‡$ = 17.8 kcal/mol, pathway A) and six-coordinate ($\Delta G^‡$ = 18.0 kcal/mol, pathway B) mechanisms. However, the pathway B transition structure exhibits a significantly lengthened Pd···N distance *trans* to the site of nucleophilic attack (Pd···N^3 = 2.937 Å, for X = SPh). This long Pd···N distance appears to represent a weak interaction (sum of van der Waals radii M + N = 3.18 Å).[35] Wiberg Bond Indices (WBI) were computed to compare the Pd–N^1 and Pd–N^2 bonds (*trans* to CF_3 (0.345) and Ph (0.368)) with the Pd···N^3 interaction (0.132). These values are consistent with a five-coordinate-like transition state in the "pathway B" Pd system.

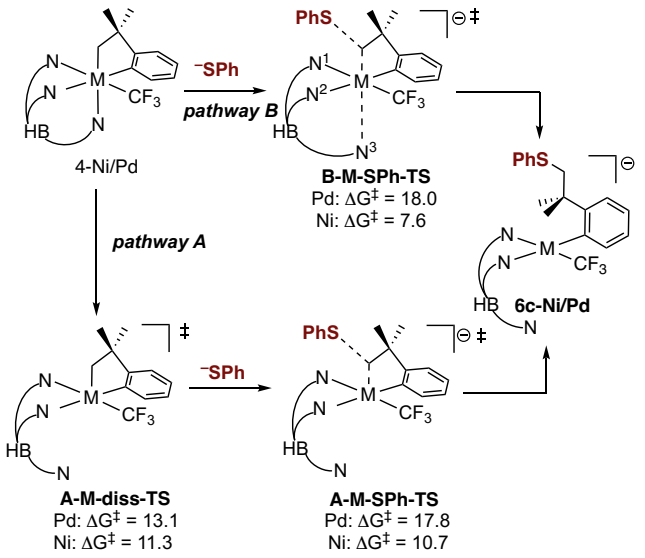

Figure 10. Energy schemes for the reaction of thiophenoxide with **4-Ni** and **4-Pd** via a five-coordinate intermediate (pathway A), or direct nucleophilic attack (pathway B). For nickel, the barrier for the five-coordinate mechanism is determined by the TS for dissociation of the axial pz group **A-Ni-diss-TS** as shown in Figure 9; the barrier for ⁻SPh attack is 10.7 kcal/mol. Energies ΔG in kcal/mol.

In contrast, for Ni, the six-coordinate mechanism (pathway B, Figure 10) is clearly the lower energy pathway, with a $\Delta\Delta G^{\ddagger}$ 3.7 kcal/mol. In this case, the Ni···N bond distances are significantly shorter than those at Pd, resulting in comparatively larger Wiberg Bond Indices (e.g. 2.603 Å and 0.165 for X = SPh, Ni···N^3). These data are consistent with a more "six-coordinate-like" transition state in the Ni system (see Table S4 for full details). As discussed above, this represents an unusual example of direct C(sp^3)–X coupling at an octahedral group 10 metal center.[34] We attribute this pathway to the highly electrophilic Ni^{IV}–alkyl carbon, which renders direct attack by the strongly nucleophilic ⁻SPh to be lower in energy than pyrazole dissociation.

Reactivity and Mechanism of M^{II}-Alkyl Azides. A final set of experimental and computational studies focused on the distinct reactivity of tetrabutylammonium azide (NBu_4N_3). The treatment of **4-Ni** with 1 equiv of NBu_4N_3 initially led to the formation of Ni^{II} alkyl azide **6d-Ni** (Scheme 6). This product can be detected by NMR spectroscopic analysis of the crude reaction mixture. However, it reacts within 15 h at room temperature to extrude N_2 and form 3,3-dimethylindoline via Ni^{II} intermediate **7**.[36] In contrast, the corresponding Pd^{II} complex **6d-Pd** is remarkably stable, with no decomposition or indoline product observed even upon heating at 70 °C for several weeks.

Scheme 6. Distinct reactivity of M^{II}–alkyl azides **6d-Ni** and **6d-Pd**.

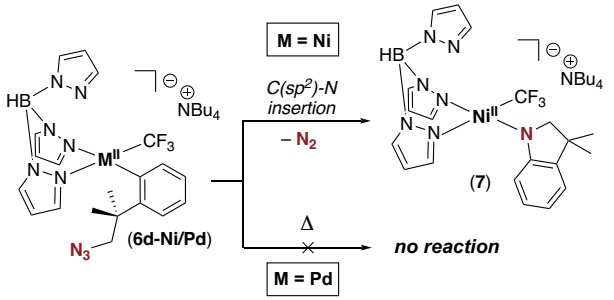

We turned to DFT calculations to better understand the reactivity differences between **6d-Ni** and **6d-Pd**. The mechanism for the conversion of **6d-Ni** to Ni^{II} intermediate **7** was explored using CAM-B3LYP.[37] A first pathway identified for the conversion of **6d-Ni** to **7** involves a singlet open shell mechanism with a Ni^{IV}-imido intermediate (Figure 11, blue profile). This pathway proceeds via the formation of an initial weak Ni···N interaction to generate intermediate **S-I**. The highest energy transition structure (**S-TS-I**) involves the transformation of **S-I** to a Ni^{IV}–imido complex **S-III**, with a barrier of 38.4 kcal/mol. Complex **S-III** can then undergo C(sp^2)–N coupling to generate **7**.

An alternative reaction manifold involving triplet intermediates was found to be substantially lower in energy ($\Delta\Delta G^{\ddagger}$ = 9.2 kcal/mol for the highest energy transition state of each process). As shown in the black profile in Figure 11, this pathway involves an initial Minimum Energy Crossing Point (MECP) from **S-I** to the triplet structure **T-II**. Intermediate **T-II** then extrudes N_2 to form the anionic nitrene intermediate (**T-III**) via triplet transition structure **T-TS-I**. This step has the highest barrier of the sequence (29.2 kcal/mol). C–N coupling from **T-III** proceeds via intermediate **T-IV** and **T-TS-II** to form intermediate **T-V**. Collapse of **T-V** to generate Ni product **7** then occurs via a second MECP (ΔE = 13.1 kcal/mol). Gaussview diagrams of the triplet species together with bonding models for these intermediates are shown in Figure 12.

The initially-formed triplet intermediate (**T-II**) has a nonlinear N^1-N^2-N^3 unit (129°) with spin density located primarily on Ni (1.09 e^-) and N^3 (0.79 e^-), consistent with a Ni^{III} formulation (Figure 12). Loss of dinitrogen gives **T-III** where the spin density is now localized primarily at N^1 (N^1 = 1.31 e^-; Ni = 0.65 e^-). As shown in Figure 12, intermediate **T-III** can be viewed as a Ni^{III} nitrene or imidyl species ($NR^{-\bullet}$)[38] in resonance with a neutral-Ni^{II} nitrene species. Structure **T-IV** can be represented similarly (N_1 = 1.15 e^-; Ni = 0.85 e^-).[38b,39] Overall, the calculations suggest that the distinct reactivity of the Ni^{II} alkyl azide **6d** results from the accessibility of the Ni^{III} oxidation state.

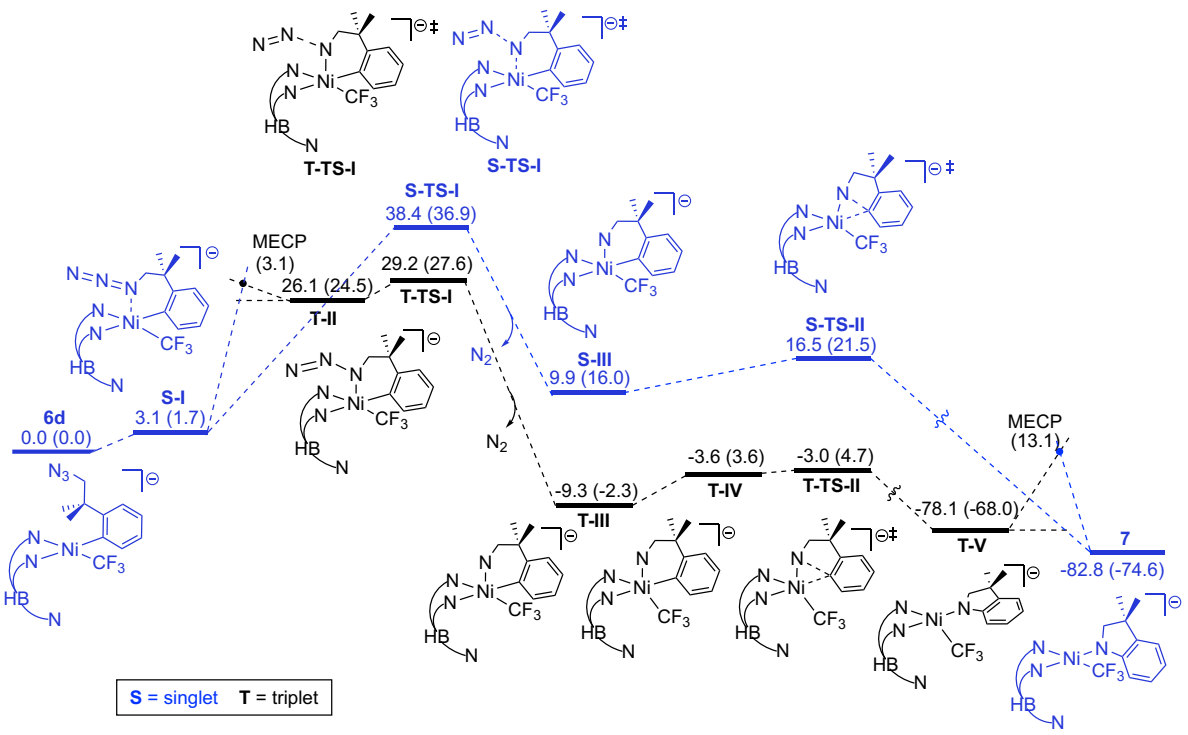

Figure 11. Energy profiles computed for the formation of Ni^{II} indolinide complexes from **6d-Ni** via singlet (blue) and triplet states (black). Energies ΔG (ΔH) in kcal/mol referenced to **6d**, except for the Minimum Energy Crossing Points (MECP) computed as ΔE 3.1 kcal/mol above **T-II**, and ΔE 13.1 kcal/mol above **T-V**, at the BS1 level.

Analogous pathways at Pd were found to involve substantially higher energy transition states than the Ni system (minimum $\Delta\Delta G^{\ddagger}$ = 6.4 kcal/mol). This is consistent with experimental studies showing that **6d-Pd** does not undergo conversion to the analogue of **7**, even after prolonged heating (Scheme 6). Interestingly, while the triplet Ni^{III} pathway was favored over the singlet Ni^{IV}-imido mechanism ($\Delta\Delta G^{\ddagger}$ = 9.2 kcal/mol), the analogous processes for Pd were indistinguishable ($\Delta\Delta G^{\ddagger}$ = 1.9 kcal/mol; Figure 13). Overall, these DFT studies show that the ability of Ni to undergo single electron chemistry leads to reactivity that is not readily accessible at the Pd analogue.

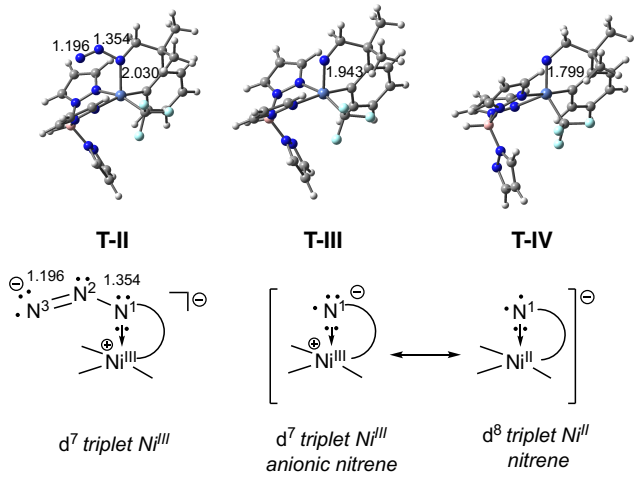

Figure 12. Gausview diagrams and bonding models of triplet intermediates **T-II**, **T-III**, and **T-IV**.

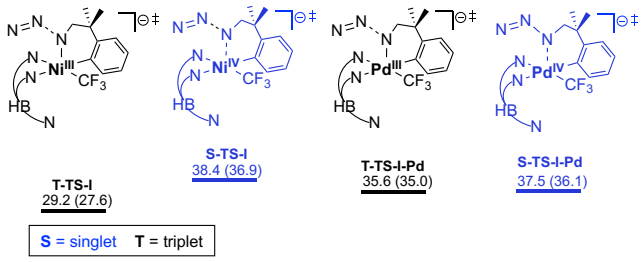

Figure 13. Transition structures computed for loss of N_2 from Ni^{II} intermediate **6d-Ni** and Pd^{II} complex **6d-Pd**. Energies $\Delta G^{\ddagger}$ ($\Delta H^{\ddagger}$) in kcal/mol referenced to **6d-Ni** or **6d-Pd**.

CONCLUSIONS

This report describes a detailed comparison of Ni^{IV} and Pd^{IV} complexes bearing identical supporting ligands. A combination of experimental and computational studies reveal many similarities in the chemistry of Ni^{IV} and Pd^{IV}, but a role for Ni^{III} in enabling reactivity that is distinct from that of palladium. In particular, electrochemical analyses and chemical oxidations of Tp-ligated M^{II} precursors demonstrate that the Ni^{IV} and Pd^{IV} species can be accessed under comparable conditions. Reactivity and mechanistic studies of isolated Ni^{IV} and Pd^{IV} complexes show that both undergo C(sp^3)–heteroatom bond-forming reactions, with the Ni system reacting under milder conditions.

In contrast to Pd, the +3 oxidation state for Ni is readily accessible.[11,40] The propensity of Pd to undergo two-electron redox chemistry and for Ni to readily promote one-electron transfer processes is confirmed via electrochemical analyses, oxidation studies monitored by NMR spectroscopy, and the distinct reactivity profiles of M^{II}-alkyl azide derivatives. Computations carried out on the latter system suggest that a Ni-mediated C(sp^2)–N insertion process occurs via a transient Ni^{III} intermediate. This pathway is not energetically accessible at the analogous Pd complex. Overall, these results demonstrate the importance of the metal and oxidation state on reactivity and selectivity. Additionally, they show the potential for similar roles of Ni^{IV}/Pd^{IV} and a complementary role for Ni^{III} in catalysis.

EXPERIMENTAL SECTION

General Procedures. All experiments and manipulations were carried out under an inert nitrogen atmosphere using standard glovebox or Schlenk techniques unless otherwise indicated. NMR spectra were obtained on a Varian VNMR 700 (699.76 MHz for ^{1}H; 175.95 MHz for ^{13}C), a Varian VNMR 500 (500.09 MHz for ^{1}H; 470.56 MHz for ^{19}F) or a Varian VNMR 400 spectrometer (399.54 MHz for ^{1}H; 128.187 for ^{11}B). ^{1}H and ^{13}C chemical shifts are reported in parts per million (ppm) relative to TMS, with the residual solvent peak as an internal reference. ^{19}F chemical shifts and ^{11}B chemical shifts are reported in ppm and are referenced on a unified scale, where the single primary reference is the frequency of the residual solvent peak in the ^{1}H NMR spectrum. Abbreviations used in the NMR data: s, singlet; d, doublet; dd, doublet of doublets; t, triplet; td, triplet of doublets; m, multiplet; br, broad signal; bq, broad quartet. Cyclic voltammetry was performed using a CHI600C potentiostat from CH instruments. The electrodes were obtained from BASi. Mass spectral data were obtained on a Micromass magnetic sector mass spectrometer in electrospray ionization mode. X-ray crystallographic data were collected on a Rigaku AFC10K Saturn 944+ CCD-based X-ray diffractometer. Flash chromatography was conducted using a Biotage Isolera One system with cartridges containing high performance silica gel. Complexes **1-Ni**,[10c] **2-Ni**,[10e] **4-Ni**,[10c] and **6a-d-Ni**[10c] were prepared from literature procedures. The NMR spectra of complex **3-Pd** was consistent with the literature report.[18]

Synthesis of NMe_4[(Tp)Pd^{II}(CH_2CMe_2-*o*-C_6H_4)] (1-Pd): A 250 mL round bottom flask was charged with (COD)Pd(CH_2CMe_2-*o*-C_6H_4) (300 mg, 0.864 mmol, 1.0 equiv). The yellow solid was dissolved in dichloromethane (50 mL) and NMe_4Tp (260 mg, 0.907 mmol, 1.1 equiv) was added at room temperature. The light tan solution was allowed to stir for 2 h. The crude reaction mixture was then concentrated to a tan solid, washed several times with ether (3 x 10 mL), and dried under vacuum to afford **1-Pd** as a white solid (404 mg; 89 % yield). ^{1}H NMR (700 MHz, CD_3CN, 23 ºC) δ 7.90 (br, 3H), 7.63 (br, 3H), 7.27 (d, J_{HH} = 7.2 Hz, 1H), 6.80 (t, J_{HH} = 7.2 Hz, 1H), 6.72 (t, J_{HH} = 7.2 Hz, 1H), 6.69 (d, J_{HH} = 7.2 Hz, 1H), 6.17 (br, 3H), 4.73 (bq, B-*H*), 3.04 (s, 12H), 1.96 (s, 2H), 1.33 (s, 6H). ^{13}C NMR (176 MHz, CD_3CN, 23 ºC) δ 168.40, 161.91, 140.44, 135.95, 134.72, 122.92, 121.46, 121.10, 103.62, 55.1, 47.31, 40.72, 33.59. ^{11}B NMR (225 MHz, CD_3CN, 23 ºC) δ –1.83 (d, J_{BH} = 112 Hz, *B*-H). HRMS-electrospray (m/z): [M–NMe_4]$^-$ calcd. for $C_{19}H_{22}BN_6Pd$, 451.1034; found, 451.1067

Synthesis of [(Tp)Ni^{IV}(CH_2CMe_2-*o*-C_6H_4)(MeCN)]BF_4 (3-Ni): In the glovebox, a 20 mL vial was charged with K[(Tp)Ni^{II}(CH_2CMe_2-*o*-C_6H_4)] (150 mg, 0.34 mmol, 1.0 equiv). The yellow solid was dissolved in acetonitrile (10 mL), and a solution of $AgBF_4$ (134 mg, 0.69 mmol, 1.0 equiv) in acetonitrile (5 mL) was added at –35 ºC. The orange solution immediately turned dark red, with concomitant precipitation of Ag^0. The crude reaction mixture was then filtered through a celite plug. The plug was washed with acetonitrile (5 mL), and the filtrates were combined and concentrated to approximately 2 mL. Red-orange crystals precipitated from the solution over the course of 15 min. These crystals were collected, washed with acetonitrile (5 mL), and dried under vacuum to afford **3-Ni** as a red-orange solid (91 mg, 51% yield). ^{1}H NMR (700 MHz, CD_3CN, 23 ºC) δ 8.18 (d, J_{HH} = 2.0 Hz, 1H), 8.13 (d, J_{HH} = 2.0 Hz, 1H), 7.99 (d, J_{HH} = 2.3 Hz, 1H), 7.97 (d, J_{HH} = 2.3 Hz, 1H), 7.86 (d, J_{HH} = 2.3 Hz, 1H), 7.26 (t, J_{HH} = 7.7 Hz, 1H), 7.19 (d, J_{HH} = 7.7 Hz, 1H), 6.94 (t, J_{HH} = 7.7 Hz, 1H), 6.77 (d, J_{HH} = 2.3 Hz, 1H), 6.74 (d, J_{HH} = 7.7 Hz, 1H), 6.55 (d, J_{HH} = 2.3 Hz, 1H), 6.49 (s, 1H), 6.22 (s, 1H), 6.09 (d, J_{HH} = 3.8 Hz, 1H), 6.00 (d, J_{HH} = 3.8 Hz, 1H), 4.61 (bq, B-*H*) 2.36 (s, 3H), 1.68 (s, 3H), 1.59 (s, 3H). ^{13}C NMR (176 MHz, CD_3CN, 0 ºC) δ 154.20, 151.08, 143.77, 141.80, 141.62, 138.08, 136.50, 136.07, 132.52, 128.97, 127.94, 127.49, 107.86, 107.15, 106.96, 87.40, 48.24, 31.38, 28.50. ^{11}B NMR (225 MHz, CD_3CN, 23 ºC) δ –1.18 (s, BF_4), –4.38 (d, J_{BH} = 98 Hz, *B*-H). ^{19}F NMR (471 MHz, CD_3CN, 23 ºC) δ –151.95. HRMS-electrospray (m/z): [M]$^+$ calcd. for $C_{21}H_{25}BN_7Ni$, 444.1612; found, 444.1613.

Synthesis of [(Tp)Pd^{IV}(CH_2CMe_2-*o*-C_6H_4)(CF_3)] (4-Pd): A 20 mL vial was charged with NMe_4[(Tp)Pd^{II}(CH_2CMe_2-*o*-

C_6H_4)] (**1-Pd**) (290 mg, 0.55 mmol, 1.0 equiv). The solid was dissolved in acetonitrile (15 mL). *S*-(Trifluoromethyl) dibenzothiophenium triflate (288 mg, 0.72 mmol, 1.3 equiv) was added at room temperature and the light tan solution immediately turned orange-brown. The solvent was removed by rotary evaporation. The crude brown solid was purified by flash chromatography on silica gel (mobile phase: ethyl acetate/hexanes with a gradient from 90:10 to 70:30). Compound **4-Pd** was isolated as a light tan solid (245 mg, 86% yield). ^{1}H NMR (700 MHz, CD_3CN, 23 ºC): δ 8.04 (d, J_{HH} = 1.9 Hz, 1H), 7.89 (d, J_{HH} = 2.3 Hz, 1H), 7.87 (d, J_{HH} = 2.3 Hz, 1H), 7.83 (d, J_{HH} = 1.9 Hz, 1H), 7.79 (d, J_{HH} = 2.3 Hz, 1H), 7.26 (m, 1H), 7.18 (m, 1H), 7.10 (dd, J_{HH} = 7.7, 1.7 Hz, 1H), 6.93 (td, J_{HH} = 7.7, 1.7 Hz, 1H), 6.86 (d, J_{HH} = 2.2 Hz, 1H), 6.42 (t, J_{HH} = 2.2 Hz, 1H), 6.38 (t, J_{HH} = 2.2 Hz, 1H), 6.14 (d, J_{HH} = 2.2 Hz, 1H), 4.63 (bq, B-*H*), 4.19–4.13 (multiple peaks, 2H), 1.51 (s, 3H), 1.50 (s, 3H). ^{13}C NMR (176 MHz, CD_3CN, 23 ºC): δ 161.23, 154.38, 141.48, 140.93, 140.40, 136.09, 136.05, 135.62, 130.95, 126.71, 126.11, 126.08, 125.85 (Pd-*C*F_3, shift for CF_3 group extracted from ^{19}F–^{13}C HMBC NMR spectrum), 105.96, 105.88, 105.72, 67.02, 45.94, 31.63, 31.53.^{19}F NMR (377 MHz, CD_3CN, 23 ºC): δ –18.39. ^{11}B NMR (225 MHz, CD_3CN, 23 ºC): δ –3.54 (d, J_{BH} = 102 Hz, *B*-H).

Synthesis of NMe_4[(Tp)Pd^{II}(C_6H_4-*o*-CMe_2CH_2OPh)(CF_3)] (6a-Pd): A 20 mL vial equipped with a magnetic stir bar was charged with [(Tp)Pd^{IV}(CH_2CMe_2-*o*-C_6H_4)(CF_3)] (**4-Pd**) (50 mg, 0.094 mmol, 1.0 equiv) and dissolved in acetonitrile (8 mL). NMe_4OPh (17 mg, 0.10 mmol, 1.1 equiv) was added and the resulting solution was stirred at 70 ºC for 32 h. The reaction mixture was cooled to room temperature, and solvent was removed by rotary evaporation. The resulting yellow residue was washed with diethyl ether (3 x 10 mL). The solids were dried under vacuum to afford complex **6a-Pd** as a yellow solid (35 mg, 56% yield). ^{1}H NMR (700 MHz, CD_3CN, 23 ºC): δ 7.89 (d, J_{HH} = 7.4 Hz, 1H), 7.77–7.66 (multiple peaks, 3H), 7.49 (d, J_{HH} = 2.3 Hz, 1H), 7.41 (s, 1H), 7.24 (d, J_{HH} = 7.9 Hz, 1H), 7.15 (t, J_{HH} = 7.9 Hz, 2H), 6.87 (t, J_{HH} = 7.5 Hz, 1H), 6.83 (t, J_{HH} = 7.5 Hz, 1H), 6.76 (d, J_{HH} = 7.8 Hz, 3H), 6.60 (s, 1H), 6.28 (s, 1H), 6.16 (s, 1H), 5.85 (s, 1H), 4.75 (bq, B-*H*) 4.35 (d, J_{HH} = 8.6 Hz, 1H), 4.26 (br, 1H), 3.07 (s, 12H), 1.78 (s, 3H), 1.47 (s, 3H). ^{13}C NMR (176 MHz, CD_3CN, 23 ºC): δ 159.80, 154.43, 150.59, 141.25, 136.98, 136.83 (Pd-*C*F_3, shift for CF_3 group extracted from ^{19}F–^{13}C HMBC NMR spectrum), 135.52, 135.20, 134.06, 129.07, 126.12, 122.56, 121.79, 119.65, 114.48, 103.90, 103.88, 103.61, 77.53, 55.18, 39.64, 27.03, 27.02. ^{11}B NMR (225 MHz, CD_3CN, 23 ºC): δ –2.04 (d, J_{BH} = 113 Hz, *B*-H). HRMS-electrospray (m/z): [M – NMe_4]$^-$ calcd. for $C_{26}H_{27}BF_3N_6PdO$, 613.1326; found, 613.1344. ^{19}F NMR (471 MHz, CD_3CN, 23 ºC) δ –18.75. ^{11}B NMR (225 MHz, CD_3CN, 23 ºC): δ –2.04 (d, J_{BH} = 113 Hz, *B*-H). HRMS-electrospray (m/z): [M–NMe_4]$^-$ calcd. for $C_{26}H_{27}BF_3N_6PdO$, 613.1326; found, 613.1344.

General Procedure for Cyclic Voltammetry Studies. Cyclic voltammetry on complexes **1-Ni** and **1-Pd** were performed in a 3-electrode cell consisting of a 3 mm glassy carbon disc working electrode, a Ag/Ag^+ reference electrode with a Ag wire in a fritted chamber containing a solution of $AgBF_4$ (0.01 M) and NBu_4PF_6 (0.1 M) in acetonitrile, and a Pt wire counter electrode. A 2 mL solution of the complex (0.01 M) and NBu_4PF_6 (0.1 M) in acetonitrile was added to the electrochemical cell. Cyclic voltammetry scans were taken at 100 mV/s. After obtaining the CV for each complex, ferrocene was added as an internal reference.

Experimental Procedure for NMR Oxidation Studies: Nickel. A 4 mL vial was charged with **1-Ni** (5.0 mg, 0.0096 mmol, 1.0 equiv) and CD_3CN (0.5 mL). This light tan solution was transferred to a screw cap NMR tube. A solution of the corresponding amount of acetylferrocenium tetrafluoroborate ($AcFcBF_4$; 3.0 mg, 0.0096 mmol, 1.0 equiv or 6.0 mg, 0.0192 mmol, 2 equiv) in CD_3CN was added. The tube was quickly capped, shaken vigorously, and was analyzed by ^{1}H NMR spectroscopy after <5 min at room temperature. In the presence of 2 equiv of $AcFcBF_4$, Ni^{IV} complex **3-Ni** was formed in 95% NMR yield. In the presence of 1 equiv of $AcFcBF_4$, analysis by ^{1}H NMR and ^{11}B NMR spectroscopy revealed the formation of a paramagnetic species that we previously characterized as Ni^{III} complex **2-Ni**.[10e]

Experimental Procedure for NMR Oxidation Studies: Palladium. A 4 mL vial was charged with **1-Pd** (5.0 mg, 0.0096 mmol, 1.0 equiv), pyridine-d_5 (4 μL; 0.05 mmol; 5.2 equiv), and CD_3CN (0.5 mL). This light tan solution was transferred to a screw cap NMR tube. A solution of the corresponding amount of acetylferrocenium tetrafluoroborate ($AcFcBF_4$; 3.0 mg, 0.0096 mmol, 1.0 equiv or 6.0 mg, 0.0192 mmol, 2 equiv) in CD_3CN was added. The tube was quickly capped, shaken vigorously, and was analyzed by ^{1}H NMR spectroscopy after <5 min at room temperature. In the presence of 2 equiv of $AcFcBF_4$, Pd complex **3-Pd** was formed in approximately quantitative yield against acetylferrocene as the internal ^{1}H NMR standard. In the presence of 1 equiv of $AcFcBF_4$, Pd complex **3-Pd** was formed in approximately 50% yield against acetylferrocene as the internal ^{1}H NMR standard with 50% of unreacted **1-Pd** remaining.

General Procedure for Determining Initial Rates of C–C Coupling. In the glovebox, complex **3-Ni** or **4-Ni** (0.0059 mmol, 1.0 equiv) was added to a J-Young valve NMR tube equipped with an O-ring seal and then dissolved in CD_3CN (0.5 mL) at room temperature. DMSO (0.014 mmol, 2.4 equiv) was added as an internal proton standard. The NMR sample was taken out of the glovebox and immediately placed in liquid nitrogen/ethyl acetate bath (approximately –84 ºC). The frozen sample was then placed in the NMR spectrometer that was preheated to 70 ºC. Reductive elimination from **3-Ni** or **4-Ni** was monitored by ^{1}H NMR spectroscopy at this temperature. Concentration versus time data were acquired from the integration of the methylene proton signals of **5** and **3-Ni**/**4-Ni** with respect to the internal standard. Initial rate values were obtained from the slope of a linear-fit line corresponding to the growth of **5**.

General Procedure for Determining Initial Rates of C–X Coupling. In the glovebox, Pd^{IV} complex **4-Pd** (3.0 mg, 0.0057 mmol, 1.0 equiv) was added to a J-Young valve NMR tube equipped with an O-ring seal. The respective nucleophile, NR_4X, where X = OPh, OAc, SPh, N_3 (0.0288 mmol, 5 equiv),

along with the internal standard 4,4'-difluorobiphenyl (~ 2 mg) was weighed into a 4 mL vial and then dissolved in CD_3CN (0.5 mL). The resulting solutions were added to the NMR tube at room temperature and taken out of the glovebox. The tube was then placed into an NMR spectrometer that had been pre-heated to 60 ºC. The rates of reductive elimination were determined by monitoring the first 10-40% of the reaction progress by ^{19}F NMR spectroscopy at this temperature. Concentration versus time data were acquired from the integration of the CF_3 signals of **4-Pd** and **6-Pd** with respect to the internal standard. Initial rate values were obtained from the slope of a linear-fit line corresponding to the decay of **4-Pd** (See Figures S8-S11).

Experimental Procedure for Determining Activation Parameters of C–O Coupling. The activation parameters for C–O coupling at **4-Ni** and **4-Pd** were determined through an Eyring Plot in the temperature range of –10 to 40 ºC and 30 to 70 ºC, respectively. In the glovebox, complex **4-Ni** or **4-Pd** (0.0055 mmol, 1.0 equiv), NMe_4OPh (0.027 mmol, 5.0 equiv), and the ^{19}F NMR standard 4,4-difluorobiphenyl (~2 mg) were weighed into a 4 mL vial. CD_3CN (0.5 mL) was added at –35 ºC and the resulting solution was transferred to a J-Young valve NMR tube equipped with an O-ring seal at this temperature. The NMR tube was taken out of the glovebox and immediately flash frozen in an ethyl acetate/liquid nitrogen bath (–84 ºC). The sample was placed into an NMR spectrometer where the probe had been pre-set to the respective temperature. The rate of reductive elimination was determined by monitoring approximately the first 10% of the reaction by ^{19}F NMR spectroscopy at various temperatures. Concentration versus time data were acquired from the integration of the CF_3 signals of **4-Ni/Pd** and **6a-Ni/Pd** with respect to the internal standard. Initial rate values were obtained from the slope of a linear-fit line corresponding to the decay of the M^{IV} complexes. The activation parameters for C–O coupling were extracted from the resulting Eyring Plot. See the Supporting Information for full details.

Computational Methods. Gaussian 09[33a] was used for DFT calculations at the B3LYP level for optimization, using the Stuttgart/Dresden ECP (SDD) basis set for Pd[33b] and the 6-31G(d) basis set for other atoms (referred to as basis set BS1). Single point calculations were performed at the B3LYP-D3 level,[33c,d] utilizing the quadruple-ξ valence polarised def2-QZVP[33e] basis set on Ni and Pd along with the corresponding ECP and the 6-311+G(2d,p) basis set on other atoms (basis set BS2). All calculations were carried out for acetonitrile as solvent with the IEFPCM (SCRF) model. All thermodynamic data were calculated at the standard state (298.15 K and 1 atm) and entropy calculations were adjusted by the method proposed by Okuno.[33f] This computational procedure has been benchmarked for palladium when applied to C···C coupling from a closely related 2,2'-bipyridine (bpy) cation $[Pd^{IV}(CH_2CMe_2\text{-}o\text{-}C_6H_4\text{-}C,C')(F)(bpy\text{-}N,N')]^+$ in acetonitrile.[14d] The triflate (OTf) salt of this cation computes as $\Delta G^{\ddagger}$ 24.7 kcal/mol, compared with experimental ($\Delta G^{\ddagger}$ 23.8 kcal/mol) and different computation procedures ($\Delta G^{\ddagger}$ 23.3 kcal/mol) for a sulfonamide (Tf_2N) salt.[14d] All transition structures contained one imaginary frequency, exhibiting atom displacements consistent with the anticipated reaction pathway. The nature of transition structures was confirmed by Intrinsic Reaction Coordinate (IRC) searches, vibrational frequency calculations, and potential energy surface scans. Natural bond order analyses[41] were performed in conjunction with BS1. For studies of formation of the indolinide complex, computation for geometry optimization and single-point employed the UCAM-B3LYP and UCAM-B3LYP-D3 functionals, respectively, within the broken-symmetry unrestricted methodology to facilitate calculations for triplet and open-shell singlet configurations.[42]

ASSOCIATED CONTENT

Supporting Information

The Supporting Information is available free of charge on the ACS Publications website.

AUTHOR INFORMATION

Corresponding Author

* Allan.Canty@utas.edu.au (AJC), mssanfor@umich.edu (MSS).

Notes

The authors declare no competing financial interest.

ACKNOWLEDGMENT

This work was supported by the US National Science Foundation (CHE 1361542 and CHE 1664961 to MSS and CHE 0840456 for X-ray instrumentation) and the Australian Research Council. We also thank Dr. Jeff Kampf for solving the X-ray crystal structures of **4-Ni** and **4-Pd**.

REFERENCES

(1) For select fundamental organometallic studies at high-valent Pd, see: (a) Uson, R.; Fornies, J.; Navarro, R. *J. Organomet. Chem.* **1975**, *96*, 307–312. (b) Byers, P. K.; Canty, A. J.; Skelton, B. W.; White, A. H. *J. Chem. Soc.*, *Chem. Commun.* **1986**, 1722–1724. (c) Alsters, P. L.; Engel, P. F.; Hogerheide, M. P.; Copijn, M.; Spek, A. L.; van Koten, G. *Organometallics* **1993**, *12*, 1831–1844. (d) Markies, B. A.; Canty, A. J.; Boersma, J.; van Koten, G. *Organometallics* **1994**, *13*, 2053–2058. (e) van Asselt, R.; Rijnberg, E.; Elsevier, C. J. *Organometallics* **1994**, *13*, 706–720. (f) van Belzen, R.; Hoffmann, H.; Elsevier, C. J. *Angew. Chem., Int. Ed.* **1997**, *36*, 1743–1745. (g) Cotton, F. A.; Gu, J.; Murillo, C. A.; Timmons, D. J. *J. Am. Chem. Soc.* **1998**, *120*, 13280–13281. (h) Dick, A. R.; Kampf, J. W.; Sanford, M. S. *J. Am. Chem. Soc.*, **2005**, *127*, 12790–12791. (i) Cotton, F. A.; Koshevoy, I. O.; Lahuerta, P.; Murillo, C. A.; Sanau,

M.; Ubeda, M. A.; Zhao, Q. *J. Am. Chem. Soc.* **2006**, *128*, 13674–13675. (j) Whitfield, S. R.; Sanford, M. S. *J. Am. Chem. Soc.* **2007**, *129*, 15142–15143. (k) Racowski, J. M.; Dick, A. R.; Sanford, M. S. *J. Am. Chem. Soc.* **2009**, *131*, 10974–10983. (l) Oloo, W.; Zavalij, P. Y.; Zhang, J.; Khaskin, E.; Vedernikov, A. N. *J. Am. Chem. Soc.* **2010**, *132*, 14400–14402. (m) Vicente, J.; Arcas, A.; Julia-Hernandez, F.; Bautista, D. *Chem. Commun.* **2010**, 7253–7255. (n) Khusnutdinova, J. R.; Rath, N. P.; Mirica, L. M. *J. Am. Chem. Soc.* **2010**, *132*, 7303–7305. (o) Bercaw, J. E.; Durrell, A. C.; Gray, H. B.; Green, J. C.; Hazari, N.; Labinger, J. A.; Winkler, J. R. *Inorg. Chem.* **2010**, *49*, 1801–1810. (p) Vicente, J.; Arcas, A.; Julia-Hernandez, F.; Bautista, D. *Angew. Chem. Int. Ed.* **2011**, *50*, 6896–6899. (q) Zhao, X.; Dong, V. M. *Angew. Chem. Int. Ed.* **2011**, *50*, 932–934. (r) Racowski, J. M.; Gary, J. B.; Sanford, M. S. *Angew Chem. Int. Ed.* **2012**, *51*, 3414–3417.

(2) For select reviews on fundamental studies at Pd^{IV}, see: (a) Canty, A. J. *Acc. Chem. Res.* **1992**, *25*, 83–90. (b) Canty, A. J. *Dalton Trans.* **2009**, 10409–10417. (c) Xu, L. M.; Li, B. J.; Yang, Z.; Shi, Z. J. *Chem. Soc. Rev.* **2010**, *39*, 712–733. (d) Sehnal, P.; Taylor, R. J. K.; Fairlamb, I. J. S. *Chem. Rev.* **2010**, *110*, 824–889. (e) Vedernikov, A. N. *Top. Organomet. Chem.* **2010**, *31*, 101–121. (f) Racowski, J. M.; Sanford, M. S. *Top. Organomet. Chem.* **2011**, *35*, 61–84. (g) Vigalok, A. *Acc. Chem. Res.*, **2015**, *48*, 238–247. (h) Desnoyer, A.; Love, J. A. *Chem. Soc. Rev.* **2017**, *46*, 197–238.

(3) For reviews on low-valent Pd catalysis, see: (a) Littke, A. F.; Fu, G. C. *Angew. Chem. Int. Ed.* **2002**, *41*, 4176–4211. (b) Nicolaou, K. C.; Bulger, P. G.; Sarlah, D. *Angew. Chem. Int. Ed.* **2005**, *44*, 4442–4489. (c) Sather, A. C.; Buchwald, S. L. *Acc. Chem. Res.* **2016**, *49*, 2146–2157.

(4) (a) Powers, D. C.; Ritter, T. *Nat. Chem.* **2009**, *1*, 302–308. (b) Powers, D. C.; Geibel, M. A. L.; Klein, J. M. E. N.; Ritter, T. *J. Am. Chem. Soc.* **2009**, *131*, 17050–17051. (c) Khusnutdinova, J. R.; Rath, N. P.; Mirica, L. M. *Angew. Chem. Int. Ed.* **2011**, *50*, 5532–5536. (d) Powers, D. C.; Ritter, T. *Top. Organomet. Chem.* **2011**, *35*, 129–156. (e) Martinez-Martinez, A.-J.; Chicote, M.-T.; Bautista, D.; Vicente, J. *Organometallics* **2012**, *31*, 3711–3719. (f) Powers, D. C.; Lee, E.; Ariafard, A.; Sanford, M. S.; Yates, B. F.; Canty, A. J.; Ritter, T. *J. Am. Chem. Soc.* **2012**, *134*, 12002–12009. (g) Tang, F.; Qu, F.; Khusnutdinova, J. R.; Rath, N. P.; Mirica, L. M. *Dalton Trans.* **2012**, *41*, 14046–14050. (h) Mirica, L. M.; Khusnutdinova, J. R. *Coord. Chem. Rev.* **2013**, *257*, 299–314. (i) Luo, J.; Rath, N. P.; Mirica, L. M. *Organometallics* **2013**, *32*, 3343–3353. (j) Canty, A. J.; Sanford, M. S.; Ariafard, A.; Yates, B. F. *Organometallics* **2013**, *32*, 544–555.

(5) For select reviews on Pd^{IV} in catalysis, see: (a) Muñiz, K. *Angew. Chem. Int. Ed.* **2009**, *48*, 9412–9423. (b) Lyons, T.; Sanford, M. S. *Chem. Rev.* **2010**, *110*, 1147–1169. (c) Hickman, A. J.; Sanford, M. S. *Nature* **2012**, *484*, 177–185. (d) Engle, K. M.; Mei, T.-S.; Wasa, M.; Yu, J.-Q. *Acc. Chem. Res.* **2012**, *45*, 788–802. (e) Topczewski, J. T.; Sanford, M. S. *Chem. Sci.* **2015**, *6*, 70–76.

(6) For select reviews, see: (a) Meijere, A. d.; Diederich, F. *Metal-Catalyzed Cross-Coupling Reactions*; Wiley-VCH: Weinheim, 2004. (b) Hu, X. *Chem. Sci.* **2011**, *2*, 1867–1886. (c) Rosen, B. M.; Quasdorf, K. W.; Wilson, D. A.; Zhang, N.; Resmerita, A-M.; Garg, N. K.; Percec, V. *Chem Rev.* **2011**, *111*, 1346–1416. (d) Montgomery, J. "Organonickel Chemistry" in *Organometallics in Synthesis: Fourth Manual* Lipshutz, B. H. (Ed.) Wiley, Hoboken, N.J., **2013**, pp. 319–428. (e) Tasker, S. Z.; Standley, E. A.; Jamison, T. F. *Nature* **2014**, *509*, 299–309. (f) Everson, D. A.; Weix, D. J. *J. Org. Chem.* **2014**, *79,* 4793–4798. (g) Ananikov, V. P. *ACS Catal.*, **2015**, *5*, 1964–1971.

(7) (a) Zultanski, S. L.; Fu, G. C. *J. Am. Chem. Soc*. **2013**, *135,* 624–627. (b) Iwasaki, T.; Kambe, N. *Top. Curr. Chem*. **2016**, *374*, 66. (c) Serrano, E.; Martin, R. *Angew. Chem. Int. Ed.* **2016**, *55,* 11207–11211. (d) Chu, C. K.; Liang, Y.; Fu. G. C. *J. Am. Chem. Soc.* **2016**, *138*, 6404–6407.

(8) (a) Dankwardt, J. W. *Angew. Chem. Int. Ed.* **2004**, *43*, 2428–2432. (b) Rosen, B. M.; Quasdorf, K. W.; Wilson, D. A.; Zhang, N.; Resmerita, A-M.; Garg, N. K.; Percec, V. *Chem. Rev*. **2011**, *111*, 1346–1416. (c) Li, B.-J.; Yu, D.-G.; Sun, C.-L.; Shi, Z.-J. *Chem. Eur. J*. **2011**, *17*, 1728–1759. (d) Chatani, N. *Top. Curr. Chem*. **2016**, *374*, 41.

(9) Rare example of Pd-catalyzed cross-coupling of alkyl bromides: Peacock, D. M.; Roos, C. B.; Hartwig, J. F. *ACS Cent. Sci.* **2016**, *2*, 647–652.

(10) (a) Higgs, A. T.; Zinn, P. J.; Sanford, M. S. *Organometallics* **2009**, *28*, 6142–6144. (b) Higgs, A. T.; Zinn, P. J.; Sanford, M. S. *Organometallics* **2010**, *29*, 5446–5449. (c) Camasso, N. M.; Sanford, M. S. *Science* **2015**, *347*, 1218–1220. (d) Bour, J. R.; Camasso, N. M.; Sanford, M. S. *J. Am. Chem. Soc.* **2015**, *137*, 8034–8037. (e) Bour, J. R.; Camasso, N. M.; Meucci, E. A.; Kampf, J. W.; Canty, A. J.; Sanford, M. S. *J. Am. Chem. Soc.* **2016**, *138*, 16105–16111. (f) Meucci, E. A.; Camasso, N. M.; Sanford, M. S. *Organometallics* **2017**, *36*, 247–250. (g) Chong, E.; Kampf, J. W.; Ariafard, A.; Canty, A. J.; Sanford, M. S. *J. Am. Chem. Soc.* **2017**, *139*, 6058–6061.

(11) For studies on Ni^{III} chemistry, see: (a) Grove, D. M.; van Koten, G.; Zoet, R.; Murrall, N. W.; Welch, A. J. *J. Am. Chem. Soc.* **1983**, *105*, 1379–1380. (b) Grove, D. M.; van Koten, G.; Mul, W. P.; van der Zeijden, A. A. H.; Terheijden, J. *Organometallics* **1986**, *5*, 322–326. (c) Grove, D. M.; van Koten, G.; Mul, P.; Zoet, R.; van der Linden, J. G. M.; Letgers, J.; Schmitz, J. E. J.; Murral, N. W.; Welch, A. J. *Inorg. Chem.* **1988**, *27*, 2466–2473. (d) van de Kuil, V. A.; Veldhuizen, Y. S. J.; Grove, D. M.; Zwikker, J. L.; Jenneskens, L. W.; Drenth, W.; Smeets, W. J. J.; Spek A. L.; van Koten, G. *J. Organomet. Chem.* **1995**, *488*, 191–197. (e) Pandarus, V.; Zargarian, D. *Organometallics* **2007**, *26*, 4321. Castonguay, A.; Beauchamp, A.; Zargarian, D. *Organometallics* **2008**, *27*, 5723–5732. (f) Lee, C.-M.; Chen, C.-H.; Liao, F.-X.; Hu, C.-H.; Lee, G.-H. *J. Am. Chem. Soc.* **2010**, *132*, 9256–9258. (g) Lipschutz, M. I.; Yang, X.; Chatterjee, R.; Tilley, T. D. *J. Am. Chem. Soc.* **2013**, *135*, 15298–15301. (h) Zhang, C.-P.; Wang, H., Klein, A.; Biewer, C.; Stirnat, K.; Yamaguchi, Y.; Xu, L..; Gomez-Benitez, V.; Vicic, D. A. *J. Am. Chem. Soc.* **2013**, *135*, 8141–8144. (i) Breitenfeld, J.; Woodrich, M.; Hu, X. *Organometallics* **2014**, *33*, 5708–5715. (j) Zheng, B.; Tang, F.; Luo, J.; Schultz, J. W.; Rath, N. P.; Mirica, L. M. *J. Am. Chem. Soc.* **2014**, *136*, 6499–6504. (k) Tang, F.; Rath, N. P.; Mirica, L. M. *Chem. Commun.* **2015**, *51*, 3113–3116. (l) Yu, S.; Dudkina, Y.; Wang, H.; Kholin, K. V.; Budnikova,

V.; Vicic, D. A. *Dalton Trans.* **2015**, *44*, 19443–19446. (m) Cloutier, J.-P.; Vabre, B.; Moungang-Soumé, B.; Zargarian, D. *Organometallics* **2015**, *34*, 133–145. (n) Zhou, W.; Schultz, J. W.; Rath, N. P.; Mirica, L. M. *J. Am. Chem. Soc.* **2015**, *137*, 7604–7607. (o) Zhou, W.; Rath, N. P.; Mirica, L. M. *Dalton Trans.* **2016**, *45*, 8693–8695. (p) Xu, H.; Diccianni, J. B.; Katigbak, J.; Hu, C.; Zhang, Y.; Diao, T. *J. Am. Chem. Soc.* **2016**, *138*, 4779–4786. (q) Schultz, J. W.; Fuchigami, K. Zheng, B. Rath, N. P.; Mirica, L. M. *J. Am. Chem. Soc.* **2016**, *138*, 12928–12934. (r) Zhou, W.; Zheng, S. A.; Schultz, J. W.; Rath, N. P.; Mirica, L. M. *J. Am. Chem. Soc.* **2016**, *138*, 5777–5780. (s) Lee, H.; Börgel, J.; Ritter, T. *Angew. Chem. Int. Ed.* **2017**, *56*, 6966–6969.

(12) For studies on Ni^{IV}chemistry, see: (a) Klein, H.-F.; Bickel haupt, A.; Jung, T.; Cordier, G. *Organometallics* **1994**, *13*, 2557–2559. (b) Klein, H. F.; Bickelhaupt, A.; Lemke, M.; Sun, H. J.; Brand, A.; Jung, T.; Rohr, C.; Florke, U.; Haupt, H. J. *Organometallics* **1997**, *16*, 668–676. (c) Shimada, S.; Rao, M. L. N.; Tanaka, N. *Organometallics* **1999**, *18*, 291–293. (d) Dimitrov, V.; Linden, A. *Angew. Chem., Int. Ed.* **2003**, *42*, 2631–2633. (e) Carnes, M.; Buccella, D.; Chen, J. Y. C.; Ramirez, A. P.; Turro, N. J.; Nuckolls, C.; Steigerwald, M. *Angew. Chem. Int. Ed.* **2009**, *48*, 290–294. (f) Martinez, G. E.; Ocampo, C.; Park, Y. J.; Fout, A. R. *J. Am. Chem. Soc.* **2016**, *138*, 4290–4293. (g) Watson, M. B.; Rath, N. P.; Mirica, L. M. *J. Am. Chem. Soc.* **2017**, *139*, 35–38. (h) Padamati, S. K.; Angelone, D., Draksharapu, A.; Primi, G.; Martin, D. J.; Tromp, M.; Marcel Swart, M.; Browne, W. R. *J. Am. Chem. Soc.* **2017**, *139*, 8718–8724. (i) D'Accriscio, F.; Borja, P.; Saffon-Merceron, N.; Fustier-Boutignon, M.; Mézailles, N.; Nebra, N. *Angew. Chem., Int. Ed.* **2017**, ASAP (DOI: 10.1002/anie.201706237)

(13) (a) Lin, B.-L.; Liu, L.; Fu, Y.; Luo, S.-W.; Chen, Q.; Guo, Q.-X. *Organometallics* **2004**, *23*, 2114–2123. (b) Ackerman, L. K. G.; Lovell, M. M.; Weix, D. J. *Nature* **2015**, *524*, 454–457.

(14) (a) Maleckis, A.; Sanford, M. S. *Organometallics* **2011**, *30*, 6617–6627. (b) Pérez-Temprano, M. H.; Racowski, J. M.; Kampf, J. W.; Sanford, M. S. *J. Am. Chem. Soc.* **2014**, *136*, 4097–4100. (c) Camasso, N. M.; Pérez-Temprano, M. H.; Sanford, M. S. *J. Am. Chem. Soc.* **2014**, *136*, 12771–12775. (d) Pendleton, I. M.; Pérez-Temprano, M. H.; Sanford, M. S.; Zimmerman, P. M. *J. Am. Chem. Soc.* **2016**, *138*, 6049–6060. (e) Canty, A. J.; Ariafard, A.; Camasso, N. M.; Higgs, A. T.; Yates, B. F.; Sanford, M. S. *Dalton Trans.* **2017**, *46*, 3742–3748.

(15) (a) O'Reilly, S. A.; White, P. S.; Templeton, J. L. *J. Am. Chem. Soc.* **1996**, *118*, 5684–5689. (b) Canty, A. J.; Dedieu, A.; Jin, H.; Milet, A.; Richmond, M. K. *Organometallics* **1996**, *15*, 2845–2847. (c) Canty, A. J.; Jin, H.; Penny, J. D. *J. Organomet. Chem.* **1999**, *573*, 30–35. (d) Reinartz, S.; White, P. S.; Brookhart, M.; Templeton, J. L. *J. Am. Chem. Soc.* **2001**, *123*, 6425–6426. (e) Campora, J.; Palma, P.; del Rio, D.; Carmona, E. *Organometallics* **2003**, *22*, 3345–3347. (f) Campora, J.; Palma, P.; del Rio, D.; Lopez, J. A.; Valerga, P. *Chem. Commun.* **2004**, 1490–1491. (g) Qu, F.; Khusnutdinova, J. R.; Rath, N. P.; Mirica, L. M. *Chem. Commun.* **2014**, *50*, 3036–3039.

(16) Tellers, D. M.; Skoog, S. J.; Bergman, R. G.; Gunnoe, T. B.; Harman, W. D. *Organometallics* **2000**, *19*, 2428–2432.

(17) Jude, H.; Krause Bauer, J. A.; Connick, W. B. *J. Am. Chem. Soc.* **2003**, *125*, 3446–3447.

(18) Campora, J.; Palma, P.; del Rio, D.; Lopez, J. A.; Alvarez, E.; Connelly, N. G. *Organometallics* **2005**, *24*, 3624–3628.

(19) (a) Albright, T. A. *Tetrahedron* **1982**, *38*, 1339–1388. (b) Albright, T. A.; Burdett, J. K. Whangbo, M.-H. *Orbital Interactions in Chemistry*, 2nd ed.; Wiley: Hoboken, NJ, 2013; pp 401−463. (c) Miessler, G. L.; Fischer, P. J.; Tarr, D. A. *Inorganic Chemistr*y, 5th ed.; Pearson/Prentice Hall: Upper Saddle River, NJ, 2014; pp 365− 382.

(20) Geiger, W. E. *Organometallics* **2007**, *26*, 5738–5765.

(21) Connelly, N. G.; Geiger, W. E. *Chem. Rev.* **1996**, *96*, 877–910.

(22) Complex **2-Ni** was fully characterized by NMR, EPR, and X-ray spectroscopy, as well as elemental analysis.

(23) For isolation and complete characterization of **3-Ni**, complex **1-Ni** was treated with 2 equiv of $AgBF_4$ and filtered through celite. This complex was isolated in 51% yield after recrystallization from acetonitrile. See the Supporting Information for full details.

(24) The ^{1}H NMR spectrum of **3-Pd** is consistent with that reported in the literature (see ref. 18).

(25) Hartwig, J. *Organotransition Metal Chemistry: From Bonding to Catalysis*. University Science Books: Sausalito, 2010.

(26) (a) Ye Y.; Ball, N. D.; Kampf, J. W.; Sanford, M. S. *J. Am. Chem. Soc.* **2010**, 132, 14682–14687. (b) Ball, N. D.; Gary, J. B.; Ye Y.; Sanford, M. S. *J. Am. Chem. Soc.* **2011**, *133*, 7577–7584.

(27) The Ni^{IV}–CF_3 bond length is within the range of reported Ni^{IV}–CF_3 and Ni^{III}–CF_3 bond distances (1.912–1.969 Å). See references 10c-f and 11k.

(28) Complexes **6b-Pd** and **6d-Pd** were characterized with residual tetraalkylammonium salts in the crude reaction mixture.

(29) The preference for C(sp^3)–X coupling over potentially competing C(sp^2)–X bond-formation is consistent with all previous studies carried out in our lab with Ni and Pd complexes of general structure $M^{IV}(CH_2CMe_2$-*o*-$C_6H_4)(X)$ (see references 1r, 10c, and 14b-e). One possible explanation for this observed selectivity is the comparatively more electrophilic M^{IV}–alkyl carbon. Upon dissociation from the metal center, the nucleophile participates in an outersphere nucleophilic attack to form the C(sp^3)–X coupled product more readily than at the less electrophilic M^{IV}–aryl carbon.

(30) (a) Swain, C. G.; Scott, C. B. *J. Am. Chem. Soc.* **1953**, *75*, 141–147. (b) Pearson, R. G.; Sobel, H. R.; Songstad, J. *J. Am. Chem. Soc.* **1968**, *90*, 319–326.

(31) For studies of C(sp^3)–heteroatom reductive elimination at Pt see: (a) Luinstra, G. A.; Labinger, J. A.; Bercaw, J. E. *J. Am. Chem. Soc.* **1993**, *115*, 3004–3005. (b) Williams, B. S.; Holland, A. W.; Goldberg, K. I. *J. Am. Chem. Soc.* **1999**, *121*, 252–253. (c) Williams, B. S.; Goldberg, K. I. *J. Am. Chem. Soc.* **2001**, *123*, 2576–2587. (d) Canty, A.J.; Denney, M. C.; van Koten, G.; Skelton, B. W.; White, A. H. *Organometallics* **2004**, *23*, 5432–5439. (e) Vedernikov, A. N.; Binfield, S. A.; Zavalij, P. Y.; Khusnutdinova, J. R. *J. Am. Chem. Soc.* **2006**, *128*, 82–83. (f) Khusnutdinova, J. R.; Zavalij, P. Y.; Vedernikov, A. N. *Organometallics*, **2007**,

26, 3466–3483. (g) Pawlikowski, A. V.; Getty, A. D.; Goldberg, K. I. *J. Am. Chem. Soc.* **2007**, *129*, 10382–10393. (h) Smythe, N. A.; Grice, K. A.; Williams, B. S.; Goldberg. K. I. *Organometallics* **2009**, *28*, 277–288. (i) Khusnutdinova, J. R.; Newman, L. L.; Zavalij, P. Y.; Lam Y.-F.; Vedernikov, A. N. *J. Am. Chem. Soc.* **2008**, *130*, 2174–2175. (j) Vedernikov, A. N. *Chem. Commun.* **2009**, 4781–4790. (k) Vedernikov, A. N. *Acc. Chem. Res.* **2012**, *45*, 803–813.

(32) Gaussian 09 was used for DFT calculations at the B3LYP level for optimization, using the Stuttgart/Dresden ECP (SDD) basis set for Pd and the 6-31G(d) basis set for other atoms (referred to as basis set BS1). Single point calculations were performed at the B3LYP-D3 level, utilizing the quadruple-ξ valence polarised def2-QZVP basis set on Ni and Pd along with the corresponding ECP and the 6-311+G(2d,p) basis set on other atoms (basis set BS2). All calculations were carried out for acetonitrile as solvent with the IEFPCM (SCRF) model. Entropy calculations were adjusted by the method proposed by Okuno (ref. 34f). See the Supporting Information for full details.

(33) (a) Frisch, M. J.; Trucks, G. W.; Schlegel, H. B. Scuseria, G. E.; Robb, M. A.; Cheeseman, J. R.; Scalmani, G.; Barone, V.; Mennucci, B.; Petersson, G. A.; Nakatsuji, H.; Caricato, M.; Li, X.; Hratchian, H. P.; Izmaylov, A. F.; Bloino, J.; Zheng, G.; Sonnenberg, J. L.; Hada, M.; Ehara, M.; Toyota, K.; Fukuda, R.; Hasegawa, J.; Ishida, M.; Nakajima, T.; Honda, Y.; Kitao, O.; Nakai, H.; Vreven, T.; Montgomery, Jr. J. A.; Peralta, J. E.; Ogliaro, F.; Bearpark, M.; Heyd, J. J.; Brothers, E.; Kudin, K. N.; Staroverov, V. N.; Kobayashi, R.; Normand, J.; Raghavachari, K.; Rendell, A.; Burant, J. C.; Iyengar, S. S.; Tomasi, J.; Cossi, M.; Rega, N.; Millam, J. M.; Klene, M.; Knox, J. E.; Cross, J. B.; Bakken, V.; Adamo, C.; Jaramillo, J.; Gomperts, R.; Stratmann, R. E.; Yazyev, O.; Austin, A. J.; Cammi, R.; Pomelli, C.; Ochterski, J. W.; Martin, R. L.; Morokuma, K.; Zakrzewski, V. G.; Voth, G. A.; Salvador, P.; Dannenberg, J. J.; Dapprich, S.; Daniels, A. D.; Farkas, O.; Foresman, J. B.; Ortiz, J. V.; Cioslowski, J.; and Fox, D. J. *Gaussian 09*, revision A.02; Gaussian, Inc.: Wallingford, CT, **2009** (b) Andrae, H.; Haussermann, U.; Dolg, M.; Stoll, H.; Preuss, H. *Theor. Chim. Acta* **1990**, *77*, 123–141. (c) Ehrlich, S.; Moellmann, J.; Grimme, S. *Acc. Chem. Res*. **2013**, *46*, 916–926. (d) Antony, J.; Sure, R.; Grimme, S. *Chem. Commun*. **2015**, *51*, 1764–1774. (e) Weigend, F.; Furche, F.; Ahrlrichs, R. *J. Chem. Phys*. **2003**, *119*, 12753–12762. (f) Okuno, Y. *Chem.-Eur. J*. **1997**, *3*, 212–218.

(34) (a) K. L. Bartlett, K. I. Goldberg, W. T. Borden, *Organometallics* **2001**, *20*, 2669–2678.; (b) Michel, C.; Laio, A.; Mohamed, F.; Krack, M.; Parrinello, M.; Milet, A. *Organometallics* **2007**, *26*, 1241–1249. (c) Fu, Y.; Li, Z.; Liang, S.; Guo, Q.-X.; Liu, L. *Organometallics* **2008**, *27*, 3736–3742.

(35) Bondi, A. *J. Phys. Chem*. **1964**, *68*, 441–451.

(36) For intermolecular alkyl azide insertions into Ni^{II}–C bonds, see: Koo, K.; Hillhouse, G. L. *Organometallics* **1995**, *14*, 4421–4423.

(37) For studies of formation of the indolinide complex, com putation for geometry optimization and single-point employed the UCAM-B3LYP and UCAM-B3LYP-D3 functionals, respectively, within the broken-symmetry unrestricted methodology to facilitate calculations for triplet and open-shell singlet configurations. Further details are given in the Supporting Information.

(38) (a) Travers, M. J.; Cowles, D. C.; Clifford, E. P.; Ellison, G. B. *J. Am Chem. Soc.* **1992**, *114*, 8699–8701. (b) Ke, Z.; Cundari, T. R. *Organometallics* **2010**, *29*, 821–834.

(39) Kim, S.-J.; Hamilton, T. P.; Schaefer III, H. F. *J. Am. Chem. Soc.* **1992**, *114*, 5349–5355.

(40) For select examples of nickel catalyzed C–C and C–heteroatom coupling reactions invoking Ni^{III} intermediates, see: (a) Jones, G. D.; Martin, J. L.; McFarland, C.; Allen, O. R.; Hall, R. E.; Haley, A. D.; Brandon, R. J.; Konovalova, T.; Desrochers, P. J.; Pulay, P.; Vicic, D. A. *J. Am. Chem. Soc.* **2006**, *128*, 13175–13183. (b) Zultanski, S.; Fu, G. C. *J. Am. Chem. Soc.* **2011**, *133*, 15362–15364. (c) Hu, X. *Chem. Sci.* **2011**, *2*, 1867–1886. (d) Joshi-Pangu, A.; Wang, C-Y.; Biscoe, M. R. *J. Am. Chem. Soc.* **2011**, *133*, 8478–8481. (e) Dudnik, A. S.; Fu, G. C. *J. Am. Chem. Soc.* **2012**, *134*, 10693–10697. (f) Dai, Y. J.; Wu, F.; Zang, Z. H.; You, H. Z.; Gong, H. G. *Chem. Eur. J.* **2012**, *18*, 808–812. (g) Schley, N. D.; Fu, G. C. *J. Am. Chem. Soc.* **2014**, *136*, 16588. (h) Aihara, Y.; Tobisu, M.; Fukumoto, Y.; Chatani, N. *J. Am. Chem. Soc.* **2014**, *136*, 15509–15512. (i) Wu, X.; Zhao, Y.; Ge, H. *J. Am. Chem. Soc.* **2014**, *136*, 1789–1792. (j) Tellis, J. C.; Primer, D. N.; Molander, G. A. *Science* **2014**, *345*, 433–436. (k) Zuo, Z.; Ahneman, D. T.; Chu, L.; Terrett, J. A.; Doyle, A. G.; MacMillan, D. W. C. *Science* **2014**, *345*, 437–440. (l) Cornella, J.; Edwards, J. T.; Qin, T.; Kawamura, S.; Wang, J.; Pan, C-M.; Gianatassio, R.; Schmidt, M. A.; Eastgate, M. D.; Baran, P. S. *J. Am. Chem. Soc.* **2016**, *138*, 2174–2177. (m) Gui, Y.-Y.; Sun, L.; Lu, Z.-P.; Yu, D.-G. *Org. Chem. Front.* **2016**, *3*, 522–526. (n) Shields, B. J.; Doyle, A. G. *J. Am. Chem. Soc.* **2016**, *138*, 12719–12722. (o) Vara, B. A.; Patel, N. R.; Molander, G. A. *ACS Catal.* **2017**, *7*, 3955–3959.

(41) Glendening, E. D.; Read, A. E.; Carpenter, J. E.; Weinhold, F. *NBO*, version 3.1; Gaussian Inc.; Pittsburgh, PA, **2003**.

(42) (a) Yanai. T.; Tew, D. P.; Handy, N. C. *Chem. Phys. Lett*. **2004**, *393*, 51–57. (b) Cramer, C. J.; Truhlar, D. G. *Phys. Chem. Chem. Phys*. **2009**, *11*, 10757–10816. (c) Poater, A.; Cavallo, L. *Theor. Chem. Acc*. **2013**, *132*, 1353.